Metabolic reprogramming and host-immune response against Crimean-Congo Hemorrhagic Fever Viruses

Short title: Metabolic reprogramming in CCHFV

Authors

Ujjwal Neogi[1,2, #*], Nazif Elaldi[3#], Sofia Appelberg[4], Anoop T. Ambikan[1], Emma Kennedy[5,10], Stuart Dowall[5], Binnur K. Bagci[6], Soham Gupta[1], Jimmy E. Rodriguez[7], Sara Svensson-Akusjärvi[1], Vanessa M. Monteil[1], Ákos Végvári[7], Friedemann Weber[8], Roger Hewson[5,10,11], Ali Mirazimi[1,4,9*]

Affiliations

[1]Division of Clinical Microbiology, Department of Laboratory Medicine, Karolinska Institute, ANA Futura, Campus Flemingsberg, Stockholm, Sweden.

[2]Department of Molecular Microbiology and Immunology and the Bond Life Science Center, University of Missouri, Columbia, MO 65211, USA

[3]Deptartment of Infectious Diseases and Clinical Microbiology, Medical Faculty, Cumhuriyet University, Sivas, Turkey

[4]Public Health Agency of Sweden, Solna, Sweden

[5]Public Health England, Porton Down, Salisbury, Wiltshire SP4 0JG, England.

[6]Department of Nutrition and Dietetics, Faculty of Health Sciences, Sivas Cumhuriyet University, Sivas, Turkey

[7]Division of Chemistry I, Department of Medical Biochemistry and Biophysics, Karolinska Institutet, Stockholm, Sweden

[8]Institute for Virology, FB10-Veterinary Medicine, Justus-Liebig University, Giessen, Germany

[9]National Veterinary Institute, Uppsala, Sweden

[10]Oxford Brookes University, Headington Road, Oxford OX3 0BP

[11]Faculty of Infectious & Tropical Diseases, London School of Hygiene and Tropical Medicine, Keppel Street, London, WC1E 7HT

[#]These authors contributed equally to this work

*Corresponding Authors: Ali Mirazimi (ali.mirazimi@folkhalsomyndigheten.se), Ujjwal Neogi (ujjwal.neogi@ki.se)

Abstract

The pathogenesis and host-viral interactions of the Crimean–Congo hemorrhagic fever virus (CCHFV) are convoluted and have not been evaluated previously. To understand the host immune responses against CCHFV, we have performed a global transcriptomic analysis of peripheral blood mononuclear cells from a longitudinal cohort of CCHF patients who survived and temporal untargeted proteomics analysis of CCHFV infected cells. Our results indicate that during the acute phase of CCHFV infection, the host's metabolic reprogramming towards central carbon metabolism including glycolysis/gluconeogenesis occurs. This could be regulated by the PI3K/Akt, HIF-1, FoxO, and AMPK signaling pathways and play a central role in viral replication. Moreover, key interferon stimulating genes (ISGs; ISG12, ISG15, ISG20 and MXs; Mx1 and Mx2) are activated during infection, suggesting a role for type I and II interferon-mediated antiviral mechanisms. Targeting type I interferon response through metabolic perturbation could be an attractive therapeutic intervention for CCHFV as well as aid as antiviral strategies.

Introduction

Crimean–Congo hemorrhagic fever orthonairovirus (CCHFV) is considered to be a major emerging viral threat causing an increasing number of outbreaks in several parts of the globe. CCHFV is a negative-sense RNA virus belonging to the *Nairoviridae* virus family, which causes a mild to severe viral hemorrhagic fever. Crimean–Congo hemorrhagic fever (CCHF) poses a substantial threat to public health due to its high mortality rate in humans (3–40%), modes of transmission (tick-to-human/animal, animal-to-human and human-to-human) and geographical distribution (WHO, 2020). The Ixodid ticks, especially those of the genus, *Hyalomma*, are both a vector and a reservoir for CCHFV and are highly ubiquitous with its presence in more than 40 countries (ECDC, 2020). CCHF is endemic in almost 30 countries that are widely distributed throughout sub-Saharan Africa, South-Eastern Europe, the Middle-East, Central Asia down to Pakistan, and as far as east as the Xinjiang province of Northwest China(Bente, Forrester et al., 2013, Zivcec, Scholte et al., 2016). In recent years, CCHFV outbreaks have become more frequent and have spread to new geographical areas; this has been attributed to climate changes and the spread of infected ticks by birds and the livestock trade. The presence of the CCHFV vector in Portugal, Spain, Germany, and even Sweden (Grandi, Chitimia-Dobler et al., 2020) and England (McGinley, Hansford et al., 2020) highlights the need for stricter surveillance due to the possibility of a future epidemic(Estrada-Peña, Sánchez et al., 2012).

Type-I interferon (IFN-I) is one of the first-line of antiviral innate immune defenses against viruses. Following infection, viral RNA or its replication products can induce secretion of IFN-I that subsequently stimulates interferon-stimulated genes (ISGs) in a tightly controlled signaling cascade. Thus, components of the IFN-I signaling pathway are often targeted by viruses to evade the antiviral immune response. It is known that CCHFV replication is sensitive to IFN-I (Andersson, Lundkvist et al., 2006). However, the virus is also able to delay the induction of IFN, and IFN treatment has been shown to be ineffective following establishment of infection, suggesting that CCHFV has developed mechanisms to block innate immune responses(Andersson, Karlberg et al., 2008). In a limited number of studies, CCHF patients were shown to have elevated innate immune response-associated cytokines and chemokines, of which IL-6 and TNF-α were often associated with mortality (Kaya, Elaldi et al., 2014, Korva, Rus et al., 2019, Weber & Mirazimi, 2008). CCHF was also observed to be associated with increased secretion of IFN-α2 and IFN-γ, irrespective of severity and disease fatality(Korva et al., 2019, Papa, Bino et al., 2006). The existing knowledge from in vitro studies, autopsies of CCHF patients and clinical findings suggests a regulatory mechanism of the IFN-response during

CCHFV infection and indicates that IFN stimulated genes may offer protection by inhibiting CCHFV. However, it is not known which among the more than 1000 ISGs are responsible for the IFN effect against CCHFV or how the strength of viral anti-IFN mechanisms and cytokine profiles might correlate with the virulence level of particular CCHFV strains.

Because of the sporadic nature of CCHF outbreaks in humans in the endemic regions, a lack of infrastructure, and the absence of structured studies, little is known about the pathogenesis and host-virus interactions during the acute phase of CCHF disease and associated sequelae after recovery. Understanding the host response to CCHFV is necessary to design better therapeutic and containment strategies for CCHF. Recently, systems biology studies using -omics approaches on patient material and infected cells have offered a route to elucidate potential mechanisms of the host immune response against invading viruses and disease pathogenesis, as recently reported by us in case of SARS-CoV-2 infection (Appelberg, Gupta et al., 2020).

In this study, we have applied transcriptomics and proteomics analysis to understand the host immune and cellular responses against CCHFV. We have used longitudinal blood samples collected during both the acute phase of CCHFV infection and the convalescent-phase (nearly after a year of recovery), as well as an *in vitro* infection model in Huh7 cells,. Our study is the first to provide a comprehensive understanding of the fundamental innate immune responses that modulate successful CCHFV infection.

Results

Samples and clinical data

In this study, 18 samples were collected during the acute phase of the disease with a median time of 4 days (range 1-6 days) after the onset of symptoms. By using SGS, 33% (6/18) patients were grouped into severity group 1, 61% (11/18) patients into severity group 2 and, 6% (1/18) patients into severity group 3. The median age of the patients was 49 (range: 18–79) years, and 12 (66.7%) of the patients were male. A 79-year-old male patient in severity group 3 died on the third day of hospitalization. The case-fatality-rate (CFR) for the cohort was 5.6%. Follow-up samples were collected from 12 individuals after a median duration of 54 weeks (range: 46-57 weeks) (Fig. 1a). The CCHF patient characteristics are summarized individually in Supplementary Table S1.

The impact of CCHF severity on peripheral blood transcriptome during acute infection

We first considered the effect of the SGS disease severity group on the gene expression profile at the mRNA level. The UMAP analysis using all of the genes did not show distinct differences between samples of different severity groups (Figure 1b). The heterogenous gene-expression profile was further refined by hierarchical clustering analysis of the top 500 high variable genes (Supplementary Figure S1). To specifically investigate the genes that were significantly associated with disease severity, the samples were grouped into either severity group 1 or severity groups 2 and 3. The differential gene expression (DGE) was plotted as an MA -plot, as a measure of the number of genes whose expression was consistently altered between these two groups (Figure 1c). There were 12 genes (ERG, PROM1, HP, HBD, AHSP, CTSG, PPARG, TIMP4, SMIM10, RNASE1, VSIG4, CMBL, MT1G) that were significantly upregulated in patients in severity groups 2 and 3 compared to severity group 1 (Figure 1c). However, no obvious links between these genes were noted.

Cytokine levels in severity group 1 and severity group 2 during acute CCHFV infection

Serum samples collected during the acute phase of the disease from severity group 1 (n=6) and severity group 2 (n=11) were analyzed using Luminex assay to assess the soluble marker. Of the 22 markers used for analysis, only IL-8 and GM-CSF were significantly higher in severity group 2, and a near significant upregulation was also observed with TNF-α and IL-10 compared to severity group 1 (Figure 1d). The levels of all of the rest 18 biomarkers are shown in Supplementary Figure S2. Cumulatively, the transcriptomics and cytokine array data suggest that there were no significant inflammatory differences with severity in patients who survived CCHF infection.

Transcriptomics changes in the acute phase and post-CCHF recovery

Due to the natural heterogeneity in human cohorts, we used longitudinal samples to perform differential expression analyses for each infected patient between the time of infection and approx. 1 year post-recovery (Range: 46 – 57 weeks). There were 12 patients (severity group 1: n=5; severity group 2: n= 7) available for which sampling was done both during acute infection and post-recovery. We observed a clear separation between the acute phase and the recovered phase samples using UMAP clustering (Supplementary Figure S3).

The DGE profile for the acute phase compared to the recovered phase in all patients showed an upregulation of 2891 genes and a downregulation of 2738. The complete profile is given in Supplementary Data File 1. The pathways that are significantly modulated by the upregulated

genes (FDR<0.05) are mainly related to metabolic pathways like glycolysis/gluconeogenesis, N-glycan biosynthesis and oxidative phosphorylation (OXPHOS), and antiviral pathways like the NOD-like receptor signaling pathway (Figure 2b and Supplementary Data File 2). However, the pathways related to the down-regulated genes were mainly related to antiviral defense mechanism-associated pathways including innate immune responses like Th1, Th2, and Th17, cell differentiation, the NF-kB pathways, chemokine signaling pathway, etc. (Figure 2c). Interestingly, although the HIF-1 signaling pathway was downregulated, the expression of the HIF-1 targeted genes that play a role in glycolysis/gluconeogenesis and coding for the glycolytic enzymes, Enolase 1 (ENO1) and Phosphoglucomutase 2 (PGM2) was significantly upregulated, while hexokinase 1 (HK1) were downregulated (Supplementary Data File 1). However, when we compared the acute phase with the recovered phase in severity group 1, and severity group 2 separately, there was a distinct DEG profile. In severity group 1 the differentially expressed genes were significantly fewer (n=1617, upregulated: 954 and downregulated: 663) compared to those in severity group 2 (n=4256, upregulated: 2182 and downregulated: 2074) (Figure 2d and 2e). This indicates that the disease severity had a significant effect on gene expression profiling during the acute phase. There were 1451 overlapping genes between severity group 1 and severity group 2 that were differentially up-regulated (n=882) and downregulated (n=569). Using gene ontology (GO) analysis after removal of the redundant terms using REVIGO (Supek, Bošnjak et al., 2011), the top two GO terms that were significantly upregulated were the type I interferon signaling pathway (GO:0060337) and the regulation of viral genome replication (GO:0045069) (Figure 2f).

Interferon signaling pathways in CCHFV infection:

We observed significant differences in gene expression relating to interferon signaling in both severity group 1 and severity group 2, and thus we further explored the alteration of gene expression in all the interferon signaling related pathways. To this end, we used supervised analysis with the genes that are part of 13 GO terms and are part of both type-I and type-II interferon signaling pathways (Figure 3a). Of the IFN-regulated genes, IFI27 (ISG12) showed the most robust upregulation (Figure 3b). This was further supported by the RNAscope analysis targeting the IFI27 transcript in the SW13 cell line infected with CCHFV strain IbAr10200 (Figure 3c). Among the pathways, the maximum significantly differentially expressed genes were part of cellular response to ITN-γ (GO:0071346) (n=57) followed by the Type I interferon (IFN-I) signaling pathway (GO:0060337) (n=35) (Figure 3a) and the majority of genes responsible for IFN-I signaling (89%; 31/35) were upregulated in the acute phase (Figure 3d). IFI27 has been previously shown to be upregulated specifically during virus infection and has the ability to

restrict several viral infections. Apart from this ISG20, ISG15, Mx1, Mx2 and several IFN-α-inducible proteins (IRFs) showed upregulation in the acute phase.

Quantitative temporal proteomics analysis of CCHFV infection in Huh7 cell lines:

Our transcriptomics analysis of CCHF patient samples revealed the role of interferon signaling pathways in the pathogenesis of CCHFV, with several ISGs being elevated during the acute phase of infection. To understand the global changes in the host interferome (cluster of interferon genes) during CCHFV infection, we infected Huh7 cells with CCHFV and used a time-course experiment for 24 and 48 hpi. We then performed TMT-based mass-spectrometric analysis (Figure 4a). The global proteome analysis revealed changes in several pathways that were related to metabolism and the organismal system (Figure 4b). This was in line with the changes we observed in the patient transcriptomics analysis (Figure 2b and 2c). Overall, 16 pathways were observed both in patients' transcriptomics and *in vitro* infection assays in Huh7 cells (Supplementary Figure S4).

To identify changes in the interferon landscape, we used the GO terms for the cellular response to IFN-γ (GO:0071346) and the Type I interferon signaling pathway (GO:0060337) that showed significant changes in expression in patient samples during acute infection. The overall changes in the interferome over time are represented as a heat-map in Figure 5a. The significant changes in the protein levels at different time points are represented as volcano plots (Figure 5b-c). At 24hpi, several ISGs, like Mx1, ISG20 and IFI16, that were upregulated in the acute-phase patient samples were also significantly elevated in infected Huh7 cells (Figure 5b). Mx1 retained a sustained elevation 48 hpi, and ISG15 was also significantly elevated (Figure 5c). The most interesting ISG was Mx2 that showed a suppression at 24hpi and a significant elevation at 48hpi (Figure 5d).

We have previously shown the anti-CCHF role of Mx1 and the interplay between ISG15 and CCHFV is well documented by us (Andersson, Bladh et al., 2004) and others(Scholte, Zivcec et al., 2017). We also observed induction of ISG20, a 3′-to-5′ exonuclease that showed elevation in both infected patients and infected cell lines. ISG20 has been reported to have anti-viral activity against a number of bunyaviruses(Feng, Wickenhagen et al., 2018). In order to ascertain its effect on CCHFV replication, we used doxycycline inducible stable cell lines that expressed human ISG20 and CAT protein as a control. Following infection with CCHFV at an MOI of 1 for 48 h, there was some degree of inhibition noted in the doxycycline-induced ISG20 cell line ($p=0.26$) and no inhibition was observed in the CAT control cell line (Figure 5e). Though not significant, the results are suggestive of an antiviral property of ISG20 that is dependent on the enzymatic

activity and this requires further investigation. Furthermore, there is also a possibility that the virus has evolved measures to counteract these antiviral responses. During the full course of infection, there was significant suppression of IRF3, the transcription factor for IFNβ production, indicating viral mediated evasion or delay in activation of the immune response. The time-dependent stimulation of different ISGs by CCHFV suggests differential regulation of the IFN pathway and does not rule out an IFN-I independent mechanism of activation of ISGs.

Discussion

Metabolic reprogramming during innate antiviral immune responses changes the subsequent phases of disease progression and influences the adaptive immune response. In this study, using the genome-wide transcriptomic analysis of a longitudinal patient cohort, and temporal proteomics from *in vitro* infection assays in Huh7 cells, we showed that metabolic reprogramming could facilitate optimal CCHFV replication and the antiviral mechanism of the host. Our data indicated that during the acute phase of CCHFV infection there is metabolic reprogramming of host cells towards central carbon metabolism (e.g. glycolysis/gluconeogenesis, pyruvate metabolism, citrate cycle/TCA cycle, pentose phosphate pathway etc) that could potentially be regulated by the PI3K/Akt, HIF-1, FoxO, and AMPK signaling pathways and play a central role in viral replication (Figure 6 and Supplementary Figure S5). Moreover, type I and II interferon-mediated antiviral mechanisms were also activated with elevated key antiviral ISGs (ISG12, ISG15, ISG20), and MXs (Mx1 and Mx2).

Both DNA and RNA viruses have been known to alter the host cell metabolism to promote their replication. Such metabolic changes follow similar patterns that include an alteration of the central carbon metabolism and a redirection of the carbon supply to metabolic pathways that are crucial for replication, indeed several virus-specific signatures have been observed in previous studies(Mayer, Stöckl et al., 2019). However, due to the lack of patient cohorts and the high-level of containment required for CCHFV, knowledge about host-virus interaction has been limited(Papa, Tsergouli et al., 2017) until now. The transcriptomics data on patient materials and *in vitro* cell culture assays indicated transient dysregulation of glycolysis/gluconeogenesis after CCHFV infection, which is known to promote replication in several other RNA viruses including HIV-1, rubella virus, dengue virus, rhinovirus, hepatitis C virus (HCV), influenza virus etc (Eisenreich, Rudel et al., 2019, Fontaine, Sanchez et al., 2015, Mayer et al., 2019, Smallwood, Duan et al., 2017, Thaker, Ch'ng et al., 2019). The upregulation of glycolysis/gluconeogenesis in CCHFV infection could be mediated by the HIF-1 signaling pathway, as the HIF-targeted genes coding for the key glycolytic enzymes ENO1 and PGM2 were significantly upregulated in CCHFV infected patients during the acute phase. We therefore hypothesize that during the CCHFV infection, the stabilization and subsequent activation of HIF-1 regulates the glycolysis/gluconeogenesis that is required for virus replication. This is further supported by our previous study in which exogenous nitric oxide (NO) inhibited CCHFV *in vitro* (Simon, Falk et al., 2006) NO regulates the HIF-1 via the PI3K/Akt pathway under normoxic conditions (Sandau, Faus et al., 2000). Interestingly we have observed a similar interplay of HIF-1 signaling and

PI3K/Akt signaling in SARS-CoV-2(Appelberg et al., 2020), where NO is able to suppress SARS-CoV-2 replication *in vitro*(Akaberi, Krambrich et al., 2020). The growing interest in hypoxia-induced signaling in emerging and re-emerging viruses and its relation with NO biology is expected to lead to further insights into the complex roles of NO, and to HIF signaling as a crucial feature of NO-mediated events during acute viral diseases. Several genes were significantly downregulated in the PI3K/Akt pathway during acute CCHFV infection, indicating the dysregulation of apathway that is critical for the cellular defense against invading pathogens.

Interestingly, an *in vitro* study in another *Bunyaviridae* virus, Rift valley fever virus (RVFV), identified the inhibition of the PI3K/Akt pathway by dephosphorylation of the AKT and Forkhead box protein O1 (FoxO1) (Popova, Turell et al., 2010). In our study we observed that the majority of the coding genes in the FoxO signaling pathway were downregulated by CCHFV, including the FOXO transcription factors FOXO1 and FOXO3, that can act as negative feedback regulators of the innate cellular antiviral response(Lei, Zhang et al., 2013). This could be due to the regulation of PI3K signaling as observed in the Epstein-Barr virus (EBV) infection (Shore, White et al., 2006). FoxO1 and FoxO3 also play an essential role in the immunometabolic dynamics and are important targets for glycolysis and gluconeogenesis (Lundell, Massart et al., 2019, Puigserver, Rhee et al., 2003).

Another critical signaling pathway that was downregulated during the CCHFV infection was AMP-activated protein kinase (AMPK) signaling that has an antiviral mechanism in addition to its role in regulating glycolysis/gluconeogenesis and FoxO1 transcriptional activity (Saline, Badertscher et al., 2019). Earlier *in vitro* studies showed that HCV inhibits the AMPK signaling pathway to promote viral replication, resulting in the downregulation of IFN-I signaling (Mankouri, Tedbury et al., 2010, Tsai, Chang et al., 2017). Interestingly, activation of the AMPK signaling pathway has been shown to inhibit the replication *in vitro* of the bunyavirus RVFV by inhibiting fatty acid synthesis (Moser, Schieffer et al., 2012). This indicates that modulation of the AMPK signaling could be an attractive therapeutic intervention for CCHFV infection through metabolic reprogramming or modulation of the IFN-I response.

The interferon signaling pathway plays a central role in innate immune responses against viruses and mediates stimulation of antiviral ISGs and secretion of pro-inflammatory cytokines. RIG-I has been recognized as the pathogen recognition receptor that recognizes CCHFV RNA, subsequently initiating a signaling cascade leading to secretion of IFN-I, mainly IFN-α and IFN-β (Spengler, Patel et al., 2015). The secreted IFN-I is further identified by the type I interferon (IFN-α/β) receptor (IFNAR) which initiates JAK-STAT signaling, leading to the stimulation of

ISGs. The protective role of IFN-I against CCHFV has been exemplified in mouse models, in which IFNAR$^{-/-}$ or STAT-1$^{-/-}$ mice (Bente, Alimonti et al., 2010, Zivcec, Safronetz et al., 2013) or STAT2$^{-/-}$ hamsters (Ranadheera, Valcourt et al., 2020) showed enhanced susceptibility to CCHFV infection. Even in *in-vitro* experiments, pre-treatment of cells with IFN-α was found to be inhibitory to CCHFV (Andersson et al., 2008). Though CCHFV is inhibited by the IFN - response, not many ISGs with anti CCHFV activity have been identified appart from MxA although, ISG20 and PKR have been proposed (Andersson et al., 2004) to have anti-CCHFV activity. Nevertheless, the anti-CCHFV activity of ISGs has not been characterized. Furthermore, in the STAT-1$^{-/-}$ mice model, CCHFV induced several IFN-stimulated genes in a delayed fashion (Zivcec et al., 2013). However, there are limited data on the effect of CCHFV on ISG stimulation in human samples. In humans, the role of the IFN response in CCHFV infection is noted by the fact that Toll-like receptor (8/9 or 3) polymorphism was shown to be associated with increased infection and fatality (Engin, Arslan et al., 2010). In the present study we mapped the ISGs induced during the acute phase of CCHFV infection compared to the recovered phase and observed that several ISGs related to the IFN-I pathway were upregulated (Figure 3a and 3b). We also observed that the ISGs with known or proposed anti-CCHFV activity, i.e. Mx1, ISG15 and ISG20 were upregulated.

Additionally, we observed significant upregulation of IFI27 (ISG12), IFITs, OASs and ISG15 (Figure 3b). IFI27 has been shown to have an antiviral effect on West-Nile virus (Lucas, Richner et al., 2015) but its impact on other viruses has not been well-studied. IFI27 was shown to distinguish between influenza and bacteria in respiratory infections (Tang, Shojaei et al., 2017) and is present at high levels in severe cases of Enterovirus 71 (EV71)-induced severe hand foot and mouth disease (Min, Ye et al., 2020), indicating its potential to be used as a biomarker. Though statistical significance was not reached, IFI27 twas 1.4-fold higher in severity groups 2 and 3 compared to severity group 1. Our study observed that IFI27 was highly differentially upregulated in CCHF infection; its role in controlling the infection therefore and its possibile use as a biomarker requires interrogation.

We further observed changes in the induction of ISGs during infection in a time-dependent manner *in vitro* by infecting the Huh7 cell line with CCHFV and observed several ISGs to be upregulated. Though we did not identify IFI27 in proteomics data, several ISGs including Mx1, OAS3, ISG20, ISG15, IFIT3, IFITM3, IFI16 that were upregulated in the acute phase CCHFV patient samples were observed to be also upregulated in the cell-infection model (Figure 5a-d). Among these, ISG20 has been shown to have antiviral activity against related-Bunyaviruses

(Feng et al., 2018), and we observed some degree of inhibitory activity of ISG20 on CCHFV replication (Figure 5e). Notably, Mx2 was differentially regulated in a time-dependent manner. At 24 hpi, Mx2 was significantly downregulated but it was upregulated by 48 hpi (Figure 4a, b and c), suggestive of a suppressive mechanism by the virus during early infection. The virus has evolved several mechanisms of evading the antiviral effects of the ISGs as observed in the case of ISG20 in our study, and one such mechanism is the de-ubiquitinase and de-ISGylase activity of the ovarian tumor (OTU)-protease encoded by the L1 protein (Scholte et al., 2017) that could directly inhibit ISG15 activity.

Similar to IFN-I, proinflammatory cytokines are important for effective innate immunity. CCHFV patients are known to have higher levels of plasma cytokine and chemokine compared to healthy people. Elevated levels of IL-6, IL-10 and TNF-α are most commonly associated with fatal outcomes(Ergonul, Tuncbilek et al., 2006, Korva et al., 2019, Saksida, Duh et al., 2010). A few studies have suggested that the co-elevation of IL-6 and TNF-α are strongly associated with fatality (Ergonul et al., 2006). Our study did not include samples from fatal cases and thus we performed a cytokine array and compared moderate and severe cases. Our results further confirmed the roles of TNF-α, IL-10, IL-8 and GM-CSF since these showed significant or near-significant elevation in severe cases. Korva et al., also observed significant differences in IL-10 and GM-CSF between moderate and severe cases(Korva et al., 2019). In another study by Hulva et al., changes in IL-6 and TNF-α were noted between moderate and severe cases, but no significant change in IL-8 was observed (Hülya, Yilmaz et al., 2017). Altough IL-6 is often associated with disease severity and fatality, we did not observe any significant difference in IL-6 levels.

In conclusion, our study provides a comprehensive description of the host-immune response against CCHFV that can explain viral pathogenesis. The interplay of the metabolic reprogramming and the IFN-mediated host antiviral mechanism could provide attractive options for therapeutic intervention of CCHF. The specific role of the different ISGs that were regulated during the course of infections need to be studied further to provide important clues for the development of antivirals or vaccines.

Materials and Methods

Ethics statement and biosafety

This study was approved by the Local Research Ethics Committee of the Ankara Numune Education and Research Hospital, Turkey (Protocol # 17-1338) and Regional Ethics Committee, Stockholm (Dnr. 2017-/1712-31/2). All patients and/or their relatives were informed about the purpose of the study and signed a consent form before collection. All the procedures were performed according to the local authority biosafety guidelines and biosafety level 4 (BSL4) practice.

Study design, patients, and sample collection:

We enrolled 18 adult patients (≧18 years) diagnosed with CCHF who were followed up by the clinical service of Infectious Diseases and Clinical Microbiology of Sivas Cumhuriyet University Hospital, Sivas, Turkey. Information about the patients was collected, including age, gender, date of symptoms onset, date of hospitalization, date of discharge/death, Severity Grading System (SGS) scores and severity groups, and outcome data (Supplementary Table 1). The CCHF patients were divided into three groups using the SGS scores of 1, 2 and 3(Bakir, Engin et al., 2012). Blood samples were collected on the admission day (acute stage) and from the survivors one year after their recovery. The samples were used for diagnosis and were sent to the CCHF Reference Laboratory, Ankara, Turkey (Public Health of Turkey). For the detection of CCHFV nucleic acid, a commercial real-time RT-PCR test (Altona Diagnostics®, Hamburg, Germany) was used, and for the serological diagnosis, a commercial IgM indirect immunofluorescence antibody (IFA) assay (Euroimmun®, Luebeck, Germany) was used. Patients having positive test results by PCR and/or serologic analyses were diagnosed with CCHF and such patients were included in the study. Peripheral blood mononuclear cells (PBMCs) were isolated by the modified density gradient centrifugation method. PBMCs and plasma were sent to the Public Health Agency of Sweden, Stockholm, Sweden. Serum cytokine profiling targeting 22 cytokines/chemokines was performed by Public Health England using methods as previously described (Dowall et al)(Dowall, Graham et al., 2019) Briefly, a 22 -plex customised luminex kit (Merck Millipore, Darmstadt, Germany) was designed to quantitate: Eotaxin, Granulocyte-Colony Stimulating Factor (G-CSF), Granulocyte Macrophage-Colony Stimulating Factor (GM-CSF), Interferon-alpha 2 (IFN-a2), Interferon-gamma (IFN-γ), Interleukin (IL)-10, IL-12, IL-15, IL-17a, IL-1a, IL-9, IL-1b, IL-2, IL-4, IL-5, IL-6, IL-8, IFN-γ-Inducible Protein 10 (IP-10), Monocyte Chemotactic Protein 1 (MCP-1), Macrophage Inhibitory Protein (MIP)-1a, MIP-1b and Tumour Necrosis Factor alpha (TNF-a). Two quality control samples and a standard included with the kit were prepared as per the manufacturers instructions. 25µl of each QC and standard concentration and 25µl of serum matrix solution were added to relevant wells of a 96 well plate in

duplicate. 25µl of each patient plasma sample and 25µl of assay buffer was added to relevant wells in duplicate. Custom pre-mixed beads were sonicated and vortexed and 25µl added to each test and standard/QC well. Plates were incubated overnight at 4°C. Following incubation, plates were washed twice with 200µl wash buffer using a hand held magnet. 25µl of detection antibody was added to each well and the plates incubated at room temperature for 1hr. 25µl streptavidin-phycoerythrin was added to each well for 30 minutes at room temperature. Each well was washed twice with 200µl wash buffer using a hand-held magnet and 100µl of 10% formalin added to each well: 40% w/v formaldehyde solution (Scientific Laboratory Supplies, Nottingham England) diluted 1:9 v/v with phosphate buffered saline solution (Thermo Fisher, Loughborough, England). The plate was subjected to formaldehyde fumigation prior to removal from Biosafety level (BSL)-4 facilities. At BSL2, the plates were washed twice with 200µl wash buffer and once with 200µl sheath buffer using a hand held magnet to remove formalin, prior to addition of 150µl sheath fluid to resuspend beads. A Luminex MAGPIX instrument using Exponent software (Invitrogen, Paisley, UK) was used to obtain results in the form of MFI (median fluorescence intensity), which was converted to concentration (pg/ml) using the standard curve prepared. Plate data was accepted based on negative background wells and QC data within the expected ranges.

RNA extraction and sequencing (Illumina RNAseq):

Total RNA was extracted from Trizol-treated PBMC using the Direct-zol RNA Miniprep (Zymo Research, CA, USA) according to the manufacturer's protocol, and the RNA quality was determined by Agilent RNA 6000 Pico kit on an Agilent 2100 Bioanalyzer (Agilent Technologies, Waldbronn, Germany). RNA-Seq was performed at the National Genomics Infrastructure, Science for Life Laboratory, Stockholm, Sweden, as described by us previously(Zhang, Ambikan et al., 2018).

Data processing and transcriptomics analysis:

The raw reads were first checked for quality and adapter content using the FastQC v0.11.8 (https://github.com/s-andrews/FastQC) tool. The Illumina adapter sequences found in the raw reads were trimmed using the tool Cutadapt v1.18 (Martin, 2011). The mean quality score across each base position in the cleaned reads was above Q30. The cleaned reads were then aligned against the human reference genome version GRCh38. The reference genome was obtained from the Illumina iGenomes repository. RNASeq aligner STAR v2.6.1a_08-27 was used for the alignment (Dobin, Davis et al., 2013). A gene-level read count table was generated from the alignment using featureCounts v1.6.3 (Liao, Smyth et al., 2014). The read count table was further

split into protein-coding genes and non-coding genes. There were 22,022 protein-coding genes. All the downstream analysis was performed on the protein-coding genes.

The raw read count data were first normalized to log2 transformed counts per million (CPM) to remove the library size effect from the R/Bioconductor package edgeR v3.28.1(Robinson, McCarthy et al., 2010). The distribution of all samples was then visualized after reducing the dimension of the data by applying the Uniform Manifold Approximation and Projection for Dimension Reduction (UMAP) technique using R package umap v0.2.6.0 (Leland, John et al., 2018). The reduced dimensions of the data were plotted in 2D space using R package ggplot2 v3.3.2 (Wickham, 2009). Differential gene expression analysis was performed using raw read counts of remaining samples using the R/Bioconductor package DESeq2 v1.26.0 (Love, Huber et al., 2014). Genes with adjusted p-values of less than 0.05 were considered as significantly regulated. Functional analysis of the significantly regulated genes was performed using the enrichr module of the python package GSEAPY v 0.9.16 (https://pypi.org/project/gseapy/) (Kuleshov, Jones et al., 2016, Subramanian, Tamayo et al., 2005). The total number of protein-coding genes as background and KEGG gene-set library downloaded from Enrichr web resources were used for the enrichment test for molecular pathway analysis. Pathways having adjusted p-values of less than 0.05 were regarded as significant. Gene ontology (GO) enrichment analysis was performed using the Enrichr web resource (Kuleshov et al., 2016), and the GO biological process 2018 category was selected. GO terms with adjusted p-values of less than 0.05 were considered as significant. Redundant GO terms were removed using the online tool REVIGO (Supek et al., 2011) using the following settings: allowed similarity 0.5, GO database *Homo sapiens,* and semantic similarity measure SimRel. Heatmaps were generated using the R/Bioconductor package ComplexHeatmap v2.2.0 (Gu, Eils et al., 2016). Bubble plots, MA plots, Volcanoplots, violin plots and bar plots were created using R package ggplot2 v3.3.2. Network visualization was performed using Cytoscape v3.6.1 (Shannon, Markiel et al., 2003). Venn diagrams were constructed using the online tool InteractiVenn (Heberle, Meirelles et al., 2015).

Cells and viruses:

The CCHFV strain IbAr10200 (originally isolated from *Hyalomma excavatum* ticks from Sokoto, Nigeria, in 1966) was used in this study. The SW13- ATCC®-CCL-105™ and human hepatocyte-derived cellular carcinoma cell line Huh7 was obtained from Marburg Virology Laboratory, (Philipps-Universität Marburg, Marburg, Germany) and matched the STR reference profile of Huh7(Rohde, Becker et al., 2019). CCHFV was propagated and titered in SW13 cells. The virus was serially diluted 10-fold and 100ul of each dilution was added to SW13 cells in a 96 well

plate. At 48 h post-infection (hpi), cells were fixed in ice-cold acetone-methanol (1:1) and stained using a rabbit polyclonal anti-CCHFV nucleocapsid antibody followed by a fluorescein isothiocyanate (FITC)-conjugated anti-rabbit antibody (Thermo Fisher Scientific, US) and DAPI (Roche, US). The number of fluorescent foci in each well was counted using a fluorescence microscope and the titer was determined. Human 293 FLP-IN TRex cells expressing CAT or ISG20 under the control of a Tet-on promoter were kindly provided by Ju-Tao Guo (Drexel University College of Medicine, Pennsylvania , USA).(Jiang, Weidner et al., 2010) The cells were propagated in DMEM supplemented with 5% Tet-negative FCS (PAA Lab, US).

In vitro infection assay in Huh7 cells and tandem mass tag (TMTpro) labelled reverse phase liquid chromatography mass-spectrometric (RPLC-MS/MS) analysis:

Huh7 cells were infected with the CCHFV in triplicate, as described by us previously (Appelberg et al., 2020). Briefly, Huh7 cells were infected with CCHFV IbAr10200 at a multiplicity of infection (MOI) of 1. After 1 h of incubation (37°C, 5% CO_2) the inoculum was removed, the cells were washed with PBS, and 2 ml DMEM supplemented with 5% heat-inactivated FBS was added to each well. Samples were collected in triplicate at 24 and 48 hpi along with controls. The medium was removed, cells were washed carefully with PBS and lyzed in lysis buffer, (10 mM Tris, 150 mM NaCl, 10% SDS, and protease inhibitor). After that, 4x sample buffer (ThermoFisher, US) was added and the samples were boiled at 99°C for 10 min. Protein digestion was performed in S-Trap microcolumns (Protifi, Huntington, NY) and the resulting peptides were labeled with TMTpro tags. Labeled peptides were fractionated by high pH (HpH) reversed-phase chromatography, and each fraction was analyzed on an Ultimate 3000 UHPLC (Thermo Scientific, San Jose, CA) in a 120 min linear gradient. Data were acquired on a Q Exactive HF-X mass spectrometer (Thermo Scientific, San Jose, CA) in data-dependent acquisition (DDA) mode collecting full mass spectra at 120,000 resolution in a mass range of 350 – 1400 *m/z* for a maximum injection time (IT) of 50 ms. Tandem mass spectra of the top 20 precursors were acquired with high collision energy (HCD) of 34%, resolution of 45,000 and maximum IT of 86 ms, isolating precursors with 0.7 *m/z* and applying 45s dynamic exclusion. Proteins were searched against the SwissProt human database using the search engine Mascot v2.5.1 (MatrixScience Ltd, UK) in Proteome Discoverer v2.4 (Thermo Scientific) software allowing up to two missed cleavages. The oxidation of methionine, deamidation of asparagine and glutamine, TMTpro at lysine and N-termini were set as variable modifications; while carbamidomethylation of cysteine was set as a fixed modification. The false discovery rate (FDR) was set to 1%.

Proteomics data analysis:

The raw data were first filtered to remove missing data. Proteins detected in all samples were retained for analysis resulting in 8,501 proteins in the filtered dataset. The filtered data was then normalized by applying eight different methods using R/Bioconductor package NormalyzerDE v1.4.0 (Willforss, Chawade et al., 2019). The quantile normalization was found superior to other methods and was selected for further use. Differential protein expression analysis was performed using R/Bioconductor package limma v3.42.2 (Ritchie, Phipson et al., 2015). Proteins with adjusted p-values of less than 0.05 were regarded as significant. KEGG pathway enrichment analysis of significantly regulated proteins was performed using the enrichr module of python package GSEAPY v 0.9.16.

ISG20 inhibition assay:

Tet-inducible HEK-293 FLP-IN TRex cells containing a CAT or ISG20 expression cassette were seeded on in six-well dishes and treated with doxycycline at a final concentration of 2 μg/ml and incubated for 36 h. Cells were infected with CCHFV strain IbAr10200 at an MOI of 1, and supernatants were titrated at 48 hpi by enumeration of fluorescent foci and calculation of progeny virus titers as described by us previously(Andersson et al., 2006).

RNAscope targeting IFI27 (ISG12) and CCHF:

The *RNAscope*® ISH Assays (ACD Bioscience,US) targeting IFI27 (440111, ACD Bioscience, US) and CCHFV (510621, ACD Bioscience, US) were perfomed as described previously.(Zhang, Svensson Akusjarvi et al., 2018) SW13 cells were infected with CCHFV (Ibar 10200 strain) at MOI of 0.1. After 1h, inoculum was replenished with fresh Leitbovitz medium containing 5% FBS and incubated 48h. After infection cells were fixed 30 min using ice-cold acetone. Cells were permeabilized using 0.1% Triton x-100 for 10 min at RT prior probe incubation at 40°C of IFI27 and CCHFV probes, Amp-1, Amp-2, Amp-3 and Amp-4 Alt C for 2h, 30min, 15 min, 30 min and 15 min, respectively. Cells were further stained using DAPI and coverslip attached using ProLong Gold Antifade reagent (P10144, Thermofisher). Images were acquired using Nikon Single Point scanning confocal with 60/1.4 oil objective.

Acknowledgments: The authors would like to acknowledge support from the National Genomics Infrastructure (NGI), Science for Life Laboratory, for RNAseq and Proteomics Biomedicum; and Karolinska Institute, Solna, for LC-MS/MS analysis. The computations were performed using resources provided by SNIC through the Uppsala Multidisciplinary Center for Advanced Computational Science (UPPMAX) under Project SNIC2017-550. The microscopy part of the study was performed at the Live Cell Imaging Facility, Karolinska Institute, Sweden, supported

by grants from the Knut and Alice Wallenberg Foundation, the Swedish Research Council, the Centre for Innovative Medicine, and the Jonasson Center at the Royal Institute of Technology, Sweden. The study is funded by Swedish Research Council Grants 2018-05766 and 2017-03126 to AM and 2017-01330 to UN, PHE Grant In Aid 109509 (inc. PhD studentship[EK]) and EU-H2020 CCHFVaccine to RH.

Author contributions: Conceptualization: U.N. and A.M., Methodology: U.N. N.E. A.M., A.V., F.W., and R.H., Formal analysis: A.T.A., S.A.,E.K., S.D., B.B., S.G., J.E.R, V.M.M. and S.S., Resources: U.N., A.M., F.W., and R.H., Writing (original draft): U.N., A.T.A, and S.G., Writing (review and editing): N.E., S.A., A.V., F.W., R.H., and A.M., Visualization: U.N., A.T.A, and S.S., Supervision: U.N., A.M., A.V., N.E., F.W., R.H., Project administration: U.N., N.E. and A.M., Funding acquisition: U.N., A.M., F.W., and R.H. All authors discussed the results, commented and approved the final version of the manuscript.

Conflict of interests: The authors declare no competing interests.

The Paper Explained: The pathogenesis and host-viral interactions of the Crimean–Congo hemorrhagic fever virus (CCHFV). We have performed a global transcriptomic analysis of peripheral blood mononuclear cells from a longitudinal cohort of CCHF patients who survived and temporal untargeted proteomics analysis of CCHFV infected cells. Our results indicate that during the acute phase of CCHFV infection, the host's metabolic reprogramming towards central carbon metabolism including glycolysis/gluconeogenesis occurs. This could be regulated by the anti-viral signaling pathways that play a central role in viral replication. Therefore targeting type I interferon response through metabolic perturbation could be an attractive therapeutic intervention for CCHFV as well as aid as antiviral strategies.

Data and materials availability: All data needed to evaluate the conclusions in the paper are present in the paper and/or the Supplementary Materials. Raw RNAseq data is avaible in Sequence Read Archive (SRA) with temporary id SUB8608640. The mass spectrometry proteomics data have been deposited to the ProteomeXchange Consortium via the PRIDE partner repository with the dataset identifier PXD022672. All the codes are available in GitHub (https://neogilab.github.io/CCHF-Turkey/)

References

Akaberi D, Krambrich J, Ling J, Luni C, Hedenstierna G, Järhult JD, Lennerstrand J, Lundkvist Å (2020) Mitigation of the replication of SARS-CoV-2 by nitric oxide in vitro. Redox biology 37: 101734

Andersson I, Bladh L, Mousavi-Jazi M, Magnusson KE, Lundkvist A, Haller O, Mirazimi A (2004) Human MxA protein inhibits the replication of Crimean-Congo hemorrhagic fever virus. Journal of virology 78: 4323-9

Andersson I, Karlberg H, Mousavi-Jazi M, Martínez-Sobrido L, Weber F, Mirazimi A (2008) Crimean-Congo hemorrhagic fever virus delays activation of the innate immune response. Journal of medical virology 80: 1397-404

Andersson I, Lundkvist A, Haller O, Mirazimi A (2006) Type I interferon inhibits Crimean-Congo hemorrhagic fever virus in human target cells. Journal of medical virology 78: 216-22

Appelberg S, Gupta S, Svensson Akusjarvi S, Ambikan AT, Mikaeloff F, Saccon E, Vegvari A, Benfeitas R, Sperk M, Stahlberg M, Krishnan S, Singh K, Penninger JM, Mirazimi A, Neogi U (2020) Dysregulation in Akt/mTOR/HIF-1 signaling identified by proteo-transcriptomics of SARS-CoV-2 infected cells. Emerging microbes & infections 9: 1748-1760

Bakir M, Engin A, Gozel MG, Elaldi N, Kilickap S, Cinar Z (2012) A new perspective to determine the severity of cases with Crimean-Congo hemorrhagic fever. Journal of vector borne diseases 49: 105-10

Bente DA, Alimonti JB, Shieh WJ, Camus G, Ströher U, Zaki S, Jones SM (2010) Pathogenesis and immune response of Crimean-Congo hemorrhagic fever virus in a STAT-1 knockout mouse model. Journal of virology 84: 11089-100

Bente DA, Forrester NL, Watts DM, McAuley AJ, Whitehouse CA, Bray M (2013) Crimean-Congo hemorrhagic fever: history, epidemiology, pathogenesis, clinical syndrome and genetic diversity. Antiviral research 100: 159-89

Dobin A, Davis CA, Schlesinger F, Drenkow J, Zaleski C, Jha S, Batut P, Chaisson M, Gingeras TR (2013) STAR: ultrafast universal RNA-seq aligner. Bioinformatics (Oxford, England) 29: 15-21

Dowall SD, Graham VA, Fletcher T, Hewson R (2019) Use and reliability if multiplex bead-based assays (Luminex) at Containment Level 4. Methods (San Diego, Calif) 158: 17-21

ECDC (2020) Hyalomma marginatum - Factsheet for experts, European Centre for Disease Prevention and Control. In

Eisenreich W, Rudel T, Heesemann J, Goebel W (2019) How Viral and Intracellular Bacterial Pathogens Reprogram the Metabolism of Host Cells to Allow Their Intracellular Replication. Frontiers in cellular and infection microbiology 9: 42

Engin A, Arslan S, Kizildag S, Oztürk H, Elaldi N, Dökmetas I, Bakir M (2010) Toll-like receptor 8 and 9 polymorphisms in Crimean-Congo hemorrhagic fever. Microbes and infection 12: 1071-8

Ergonul O, Tuncbilek S, Baykam N, Celikbas A, Dokuzoguz B (2006) Evaluation of serum levels of interleukin (IL)-6, IL-10, and tumor necrosis factor-alpha in patients with Crimean-Congo hemorrhagic fever. The Journal of infectious diseases 193: 941-4

Estrada-Peña A, Sánchez N, Estrada-Sánchez A (2012) An assessment of the distribution and spread of the tick Hyalomma marginatum in the western Palearctic under different climate scenarios. Vector borne and zoonotic diseases (Larchmont, NY) 12: 758-68

Feng J, Wickenhagen A, Turnbull ML, Rezelj VV, Kreher F, Tilston-Lunel NL, Slack GS, Brennan B, Koudriakova E, Shaw AE, Rihn SJ, Rice CM, Bieniasz PD, Elliott RM, Shi X, Wilson SJ (2018) Interferon-Stimulated Gene (ISG)-Expression Screening Reveals the Specific Antibunyaviral Activity of ISG20. Journal of virology 92

Fontaine KA, Sanchez EL, Camarda R, Lagunoff M (2015) Dengue virus induces and requires glycolysis for optimal replication. Journal of virology 89: 2358-66

Grandi G, Chitimia-Dobler L, Choklikitumnuey P, Strube C, Springer A, Albihn A, Jaenson TGT, Omazic A (2020) First records of adult Hyalomma marginatum and H. rufipes ticks (Acari: Ixodidae) in Sweden. Ticks and tick-borne diseases 11: 101403

Gu Z, Eils R, Schlesner M (2016) Complex heatmaps reveal patterns and correlations in multidimensional genomic data. Bioinformatics (Oxford, England) 32: 2847-9

Heberle H, Meirelles GV, da Silva FR, Telles GP, Minghim R (2015) InteractiVenn: a web-based tool for the analysis of sets through Venn diagrams. BMC bioinformatics 16: 169

Hülya Y, Yilmaz G, Kostakoglu U, Arslan M, Karahan SC, Koksal I (2017) Evaluation of Serum TNF-alpha, IL-6, IL-10, and IFN-gamma Levels in Patients with Crimean–Congo Hemorrhagic Fever. Open Forum Infectious Diseases 4: S312-S313

Jiang D, Weidner JM, Qing M, Pan XB, Guo H, Xu C, Zhang X, Birk A, Chang J, Shi PY, Block TM, Guo JT (2010) Identification of five interferon-induced cellular proteins that inhibit west nile virus and dengue virus infections. Journal of virology 84: 8332-41

Kaya S, Elaldi N, Kubar A, Gursoy N, Yilmaz M, Karakus G, Gunes T, Polat Z, Gozel MG, Engin A, Dokmetas I, Bakir M, Yilmaz N, Sencan M (2014) Sequential determination of serum viral titers, virus-specific IgG antibodies, and TNF-α, IL-6, IL-10, and IFN-γ levels in patients with Crimean-Congo hemorrhagic fever. BMC infectious diseases 14: 416

Korva M, Rus KR, Pavletič M, Saksida A, Knap N, Jelovšek M, Smrdel KS, Jakupi X, Humolli I, Dedushaj J, Petrovec M, Avšič-Županc T (2019) Characterization of Biomarker Levels in Crimean-Congo Hemorrhagic Fever and Hantavirus Fever with Renal Syndrome. Viruses 11

Kuleshov MV, Jones MR, Rouillard AD, Fernandez NF, Duan Q, Wang Z, Koplev S, Jenkins SL, Jagodnik KM, Lachmann A, McDermott MG, Monteiro CD, Gundersen GW, Ma'ayan A (2016) Enrichr: a comprehensive gene set enrichment analysis web server 2016 update. Nucleic acids research 44: W90-7

Lei CQ, Zhang Y, Xia T, Jiang LQ, Zhong B, Shu HB (2013) FoxO1 negatively regulates cellular antiviral response by promoting degradation of IRF3. The Journal of biological chemistry 288: 12596-604

Leland M, John H, Nathaniel S, Lukas G (2018) UMAP: uniform manifold approximation and projection. Journal of Open Source Software 3: 861

Liao Y, Smyth GK, Shi W (2014) featureCounts: an efficient general purpose program for assigning sequence reads to genomic features. Bioinformatics (Oxford, England) 30: 923-30

Love MI, Huber W, Anders S (2014) Moderated estimation of fold change and dispersion for RNA-seq data with DESeq2. Genome biology 15: 550

Lucas TM, Richner JM, Diamond MS (2015) The Interferon-Stimulated Gene Ifi27l2a Restricts West Nile Virus Infection and Pathogenesis in a Cell-Type- and Region-Specific Manner. Journal of virology 90: 2600-15

Lundell LS, Massart J, Altıntaş A, Krook A, Zierath JR (2019) Regulation of glucose uptake and inflammation markers by FOXO1 and FOXO3 in skeletal muscle. Molecular metabolism 20: 79-88

Mankouri J, Tedbury PR, Gretton S, Hughes ME, Griffin SD, Dallas ML, Green KA, Hardie DG, Peers C, Harris M (2010) Enhanced hepatitis C virus genome replication and lipid accumulation mediated by inhibition of AMP-activated protein kinase. Proceedings of the National Academy of Sciences of the United States of America 107: 11549-54

Martin M (2011) Cutadapt removes adapter sequences from high-throughput sequencing reads. EMBnet journal 17: pp. 10-12

Mayer KA, Stöckl J, Zlabinger GJ, Gualdoni GA (2019) Hijacking the Supplies: Metabolism as a Novel Facet of Virus-Host Interaction. Frontiers in immunology 10: 1533

McGinley L, Hansford KM, Cull B, Gillingham EL, Carter DP, Chamberlain JF, Hernandez-Triana LM, Phipps LP, Medlock JM (2020) First report of human exposure to Hyalomma marginatum in England: Further evidence of a Hyalomma moulting event in north-western Europe? Ticks and tick-borne diseases 12: 101541

Min Z, Ye Z, Gang L, Boyu D, Xueyan X (2020) IFI27 as a potential indicator for severe Enterovirus 71-infected hand foot and mouth disease. Virus research 289: 198149

Moser TS, Schieffer D, Cherry S (2012) AMP-activated kinase restricts Rift Valley fever virus infection by inhibiting fatty acid synthesis. PLoS pathogens 8: e1002661

Papa A, Bino S, Velo E, Harxhi A, Kota M, Antoniadis A (2006) Cytokine levels in Crimean-Congo hemorrhagic fever. Journal of clinical virology : the official publication of the Pan American Society for Clinical Virology 36: 272-6

Papa A, Tsergouli K, Tsioka K, Mirazimi A (2017) Crimean-Congo Hemorrhagic Fever: Tick-Host-Virus Interactions. Frontiers in cellular and infection microbiology 7: 213

Popova TG, Turell MJ, Espina V, Kehn-Hall K, Kidd J, Narayanan A, Liotta L, Petricoin EF, 3rd, Kashanchi F, Bailey C, Popov SG (2010) Reverse-phase phosphoproteome analysis of signaling pathways induced by Rift valley fever virus in human small airway epithelial cells. PloS one 5: e13805

Puigserver P, Rhee J, Donovan J, Walkey CJ, Yoon JC, Oriente F, Kitamura Y, Altomonte J, Dong H, Accili D, Spiegelman BM (2003) Insulin-regulated hepatic gluconeogenesis through FOXO1-PGC-1alpha interaction. Nature 423: 550-5

Ranadheera C, Valcourt EJ, Warner BM, Poliquin G, Rosenke K, Frost K, Tierney K, Saturday G, Miao J, Westover JB, Gowen BB, Booth S, Feldmann H, Wang Z, Safronetz D (2020) Characterization of a novel STAT 2 knock-out hamster model of Crimean-Congo hemorrhagic fever virus pathogenesis. Sci Rep 10: 12378

Ritchie ME, Phipson B, Wu D, Hu Y, Law CW, Shi W, Smyth GK (2015) limma powers differential expression analyses for RNA-sequencing and microarray studies. Nucleic acids research 43: e47

Robinson MD, McCarthy DJ, Smyth GK (2010) edgeR: a Bioconductor package for differential expression analysis of digital gene expression data. Bioinformatics (Oxford, England) 26: 139-40

Rohde C, Becker S, Krahling V (2019) Marburg virus regulates the IRE1/XBP1-dependent unfolded protein response to ensure efficient viral replication. Emerging microbes & infections 8: 1300-1313

Saksida A, Duh D, Wraber B, Dedushaj I, Ahmeti S, Avsic-Zupanc T (2010) Interacting roles of immune mechanisms and viral load in the pathogenesis of crimean-congo hemorrhagic fever. Clinical and vaccine immunology : CVI 17: 1086-93

Saline M, Badertscher L, Wolter M, Lau R, Gunnarsson A, Jacso T, Norris T, Ottmann C, Snijder A (2019) AMPK and AKT protein kinases hierarchically phosphorylate the N-terminus of the FOXO1 transcription factor, modulating interactions with 14-3-3 proteins. The Journal of biological chemistry 294: 13106-13116

Sandau KB, Faus HG, Brüne B (2000) Induction of hypoxia-inducible-factor 1 by nitric oxide is mediated via the PI 3K pathway. Biochemical and biophysical research communications 278: 263-7

Scholte FEM, Zivcec M, Dzimianski JV, Deaton MK, Spengler JR, Welch SR, Nichol ST, Pegan SD, Spiropoulou CF, Bergeron É (2017) Crimean-Congo Hemorrhagic Fever Virus Suppresses Innate Immune Responses via a Ubiquitin and ISG15 Specific Protease. Cell Rep 20: 2396-2407

Shannon P, Markiel A, Ozier O, Baliga NS, Wang JT, Ramage D, Amin N, Schwikowski B, Ideker T (2003) Cytoscape: a software environment for integrated models of biomolecular interaction networks. Genome research 13: 2498-504

Shore AM, White PC, Hui RC, Essafi A, Lam EW, Rowe M, Brennan P (2006) Epstein-Barr virus represses the FoxO1 transcription factor through latent membrane protein 1 and latent membrane protein 2A. Journal of virology 80: 11191-9

Simon M, Falk KI, Lundkvist A, Mirazimi A (2006) Exogenous nitric oxide inhibits Crimean Congo hemorrhagic fever virus. Virus research 120: 184-90

Smallwood HS, Duan S, Morfouace M, Rezinciuc S, Shulkin BL, Shelat A, Zink EE, Milasta S, Bajracharya R, Oluwaseum AJ, Roussel MF, Green DR, Pasa-Tolic L, Thomas PG (2017)

Targeting Metabolic Reprogramming by Influenza Infection for Therapeutic Intervention. Cell Rep 19: 1640-1653

Spengler JR, Patel JR, Chakrabarti AK, Zivcec M, García-Sastre A, Spiropoulou CF, Bergeron É (2015) RIG-I Mediates an Antiviral Response to Crimean-Congo Hemorrhagic Fever Virus. Journal of virology 89: 10219-29

Subramanian A, Tamayo P, Mootha VK, Mukherjee S, Ebert BL, Gillette MA, Paulovich A, Pomeroy SL, Golub TR, Lander ES, Mesirov JP (2005) Gene set enrichment analysis: a knowledge-based approach for interpreting genome-wide expression profiles. Proceedings of the National Academy of Sciences of the United States of America 102: 15545-50

Supek F, Bošnjak M, Škunca N, Šmuc T (2011) REVIGO summarizes and visualizes long lists of gene ontology terms. PloS one 6: e21800

Tang BM, Shojaei M, Parnell GP, Huang S, Nalos M, Teoh S, O'Connor K, Schibeci S, Phu AL, Kumar A, Ho J, Meyers AFA, Keynan Y, Ball T, Pisipati A, Kumar A, Moore E, Eisen D, Lai K, Gillett M et al. (2017) A novel immune biomarker IFI27 discriminates between influenza and bacteria in patients with suspected respiratory infection. The European respiratory journal 49

Thaker SK, Ch'ng J, Christofk HR (2019) Viral hijacking of cellular metabolism. BMC biology 17: 59

Tsai WL, Chang TH, Sun WC, Chan HH, Wu CC, Hsu PI, Cheng JS, Yu ML (2017) Metformin activates type I interferon signaling against HCV via activation of adenosine monophosphate-activated protein kinase. Oncotarget 8: 91928-91937

Weber F, Mirazimi A (2008) Interferon and cytokine responses to Crimean Congo hemorrhagic fever virus; an emerging and neglected viral zonoosis. Cytokine & growth factor reviews 19: 395-404

WHO (2020) Fact Sheet: Crimean Congo Haemorrhagic Fever. In World Health Organization Regional Office for Africa

Wickham H (2009) ggplot2: Elegant Graphics for Data Analysis. Springer International Publishing, New York

Willforss J, Chawade A, Levander F (2019) NormalyzerDE: Online Tool for Improved Normalization of Omics Expression Data and High-Sensitivity Differential Expression Analysis. Journal of proteome research 18: 732-740

Zhang W, Ambikan AT, Sperk M, van Domselaar R, Nowak P, Noyan K, Russom A, Sonnerborg A, Neogi U (2018) Transcriptomics and Targeted Proteomics Analysis to Gain Insights Into the Immune-control Mechanisms of HIV-1 Infected Elite Controllers. EBioMedicine 27: 40-50

Zhang W, Svensson Akusjarvi S, Sonnerborg A, Neogi U (2018) Characterization of Inducible Transcription and Translation-Competent HIV-1 Using the RNAscope ISH Technology at a Single-Cell Resolution. Frontiers in microbiology 9: 2358

Zivcec M, Safronetz D, Scott D, Robertson S, Ebihara H, Feldmann H (2013) Lethal Crimean-Congo hemorrhagic fever virus infection in interferon α/β receptor knockout mice is associated with high viral loads, proinflammatory responses, and coagulopathy. The Journal of infectious diseases 207: 1909-21

Zivcec M, Scholte FE, Spiropoulou CF, Spengler JR, Bergeron É (2016) Molecular Insights into Crimean-Congo Hemorrhagic Fever Virus. Viruses 8: 106

Figures

Fig. 1. Study design and severity group association with gene expression and cytokine profiling. (a) Overall work-flow of the data generation and analysis. **(b)** Sample distribution during the acute phase of infection in different severity groups as reported. **(c)** MA plot of differentially regulated genes during the acute phase between samples of severity group 1 and severity group 2 or 3. **(d)** Violin plot of significantly changed proteins as determined from ELISA assays.

Fig. 2. Differential gene expression and pathway analysis between acute and recovery phases. (a) Heatmap of Z-score transformed expression values of significantly regulated genes in the pair-wise comparisons namely Recovered vs Acute (overall), Recovered vs Acute (severity group 1), Recovered vs Acute (severity group 2). The columns represent the patient samples and their corresponding severity groups at different time points. The rows represent genes that are hierarchically clustered based on Euclidean distance. **(b)** KEGG pathway enrichment analysis results of genes belonging to cluster 1 of the heatmap. The bubble size and colour gradient correspond to the number of genes and adjusted P value of the enrichment test, respectively. (**c)** KEGG pathway enrichment results of genes belonging to cluster 2 of the heatmap. The bubble size and color gradient correspond to the number of genes and adjusted P value of the enrichment test, respectively. **(d)** Venn diagram of significantly up-regulated genes in Recovered vs Acute (severity group 1) and Recovered vs Acute (severity group 2) phases **(e)** Venn diagram of significantly down-regulated genes in Recovered vs Acute (severity group 1) and Recovered vs Acute (severity group 2) phases. **(f)** Gene ontology (biological process) enrichment analysis results of commonly regulated genes (882 upregulated and 569 down-regulated) from (d) and (e). the colour gradient and bubble size correspond to the gene ratio of each GO term and the adjusted P value of the enrichment test, respectively. The adjacent bar graph represents the percentage of genes upregulated or downregulated in each gene ontology term.

Fig. 3. Differentially expressed genes in interferon (IFN) signaling pathways. (a) Heatmap visualizing the expression pattern of IFN-signaling genes (including ISGs) that are significantly different between the recovered and acute phases. The columns represent the patient samples and

their corresponding severity groups at different time points. The rows represent genes hierarchically clustered based on Euclidean distance. The row annotation indicates the differential expression of genes (DEG) and presence or absence of genes in the selected GO terms. The names of genes involved in the cellular response to IFN-γ (GO:0071346) and the IFN-Isignaling (GO:0060337) are printed. **(b)** MA plot of differentially regulated genes between the recovered and acute phases. ISGs are marked. **(c)** RNAscope analysis targeting IFI27 genes in infected and non-infected cells. **(d)** Network type visualization of genes belonging to GO:0071346 and GO:0060337. The edges indicate the presence of the corresponding gene in the gene-ontology term. The node size and colour gradient corrospond to the adjusted P value of differential expression analysis and the log2 fold change, respectively.

Fig. 4. LC-MS/MS based proteomics analysis in CCHFV infected Huh7 cells. (a) General work-flow showing the sample preparation and data generation for the proteomics experiment. **(b)** Significant pathways identified by mapping proteins regulated over time to the KEGG database. The pathways are grouped into two: the first 29 pathways are metabolism related and the last 16 pathways are related to organismal systems and environmental information processing. The bubble size and colour gradient correspond to the number of proteins and adjusted P value of the enrichment test, respectively. The bar graphs represent the percentage of proteins upregulated or downregulated in each pathway as per the corresponding comparisons.

Fig. 5. Temporal dynamics of interferon stimulating genes (ISGs). (a) Heatmap of Z-score transformed expression values of proteins belonging to the cellular response to IHN-γ (GO:0071346) and the IFN-I interferon signaling pathway (GO:0060337) gene ontology terms. The columns represent the different sampls and their corresponding treatment conditions and time points. The rows represent proteins hierarchically clustered based on Euclidean distance. The row annotation indicates the presence or absence of proteins in the corresponding GO terms and log 2-fold change values in the proteomics and transcriptomics (recovered -vs- acute) experiments. **(b)** Volcano plot of ISGs visualizing the expression status of 24 h Mock and Infected (24 hpi) samples. The size and colour gradients of the dots correspond to the adjusted P values of differential expression analysis and the log2 fold change, respectively. **(c)** Volcano plot of ISGs visualizing the expression status of 48 h Mock and Infected (48 hpi). The size and colour gradient of the dots correspond to the adjusted P values of differential expression analysis and log2 fold change. respectively. **(d)** Volcano plot of ISGs visualizing the expression status of 24 hpi and 48 hpi. The size and colour gradient of the dots correspond to the adjusted P value of differential expression analysis and the log2 fold change, respectively. **(e)** HEK293-FLP-IN T-

Rex cells that conditionally express ISG20 or human CAT protein were treated with doxycycline or left untreated for 36 h, followed by infection with CCHFV at an MOI 1 for 48hours. Cell-free culture supernatants were harvested and progeny viral titers were determined by fluorescent focus-forming assay. Columns show means ± the standard deviations (n = 2). A two-tailed paired Student t test was performed to compare titers of untreated and doxycycline-treated cells.

Fig. 6. Potential host-cellular, immune response and metabolic reprogramming in CCHFV infection. The figure is created with BioRender.com.

Supplementary Materials

Supplementary Table S1. The CCHF patient characteristics.

Supplementary Figure S1: The heterogenous gene-expression profile was further refined by hierarchical clustering analysis of the top 500 high variable genes

Supplementary Figure S2. The levels of all of the rest 18 soluble marker.

Supplementary Figure S3: UMAP clustering of the caute phase and recovered phase samples.

Supplementary Figure S4: Overlap of the pathways identified between patients based transcriptomics data and in vitro cellular data.

Supplementary figure S5. Potential pathways regulated by CCHFV during acute phase of infection

Supplementary Data File 1: The DGE profile for the acute phase compared to the recovered phase in all patients showed an upregulation of 2891 genes and a downregulation of 2738

Supplementary Data File 2: The pathways that are significantly modulated by the upregulated and downregulated genes.

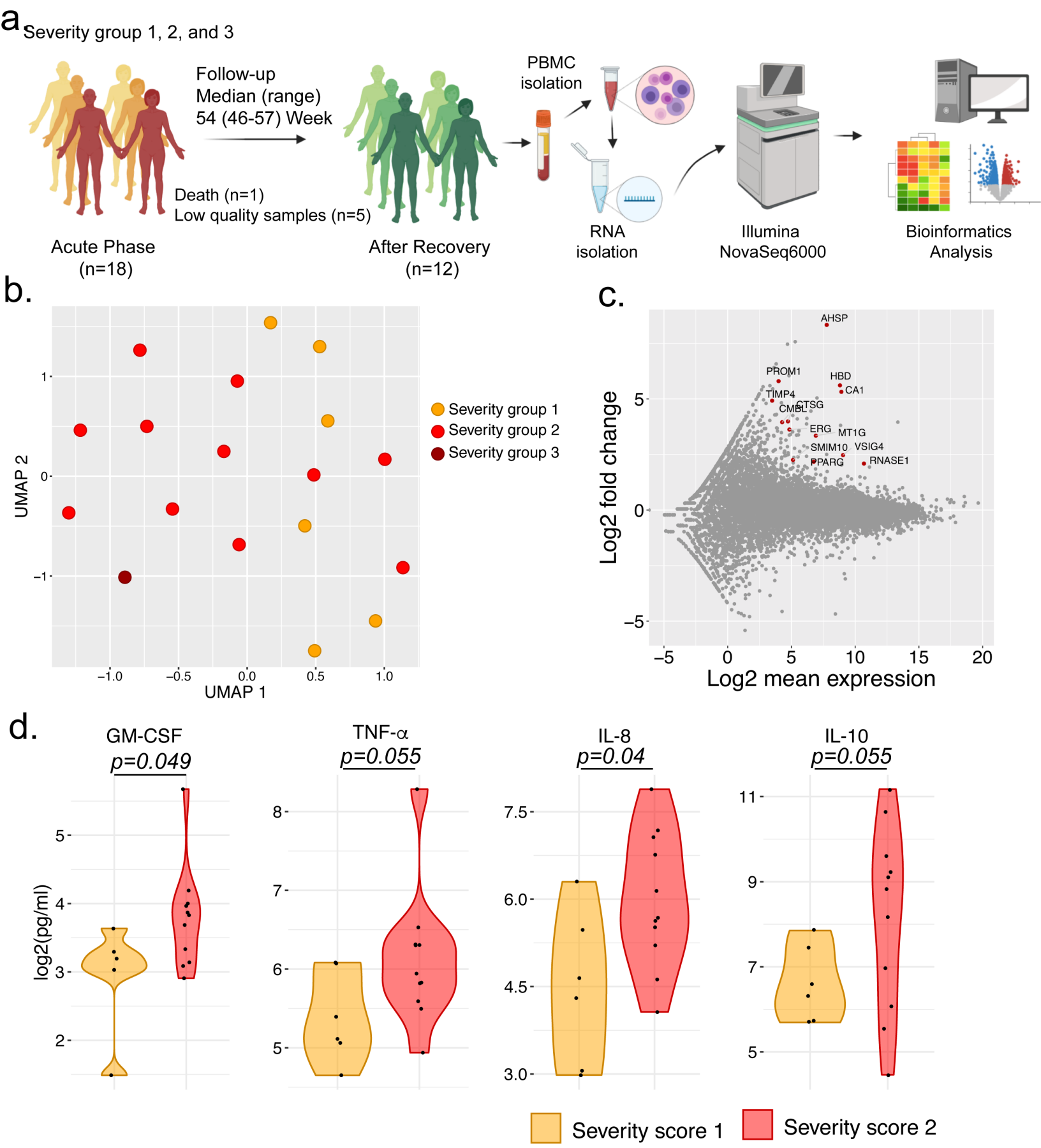
a
Severity group 1, 2, and 3
Follow-up
Median (range)
54 (46-57) Week
Death (n=1)
Low quality samples (n=5)
Acute Phase
(n=18)
After Recovery
(n=12)
PBMC
isolation
RNA
isolation
Illumina
NovaSeq6000
Bioinformatics
Analysis
b.
Severity group 1
Severity group 2
Severity group 3
UMAP 2
UMAP 1
c.
AHSP
PROM1
HBD
CA1
TIMP4
CTSG
CMBL
ERG
MT1G
SMIM10
VSIG4
PPARG
RNASE1
Log2 fold change
Log2 mean expression
d.
GM-CSF
p=0.049
TNF-α
p=0.055
IL-8
p=0.04
IL-10
p=0.055
log2(pg/ml)
Severity score 1
Severity score 2

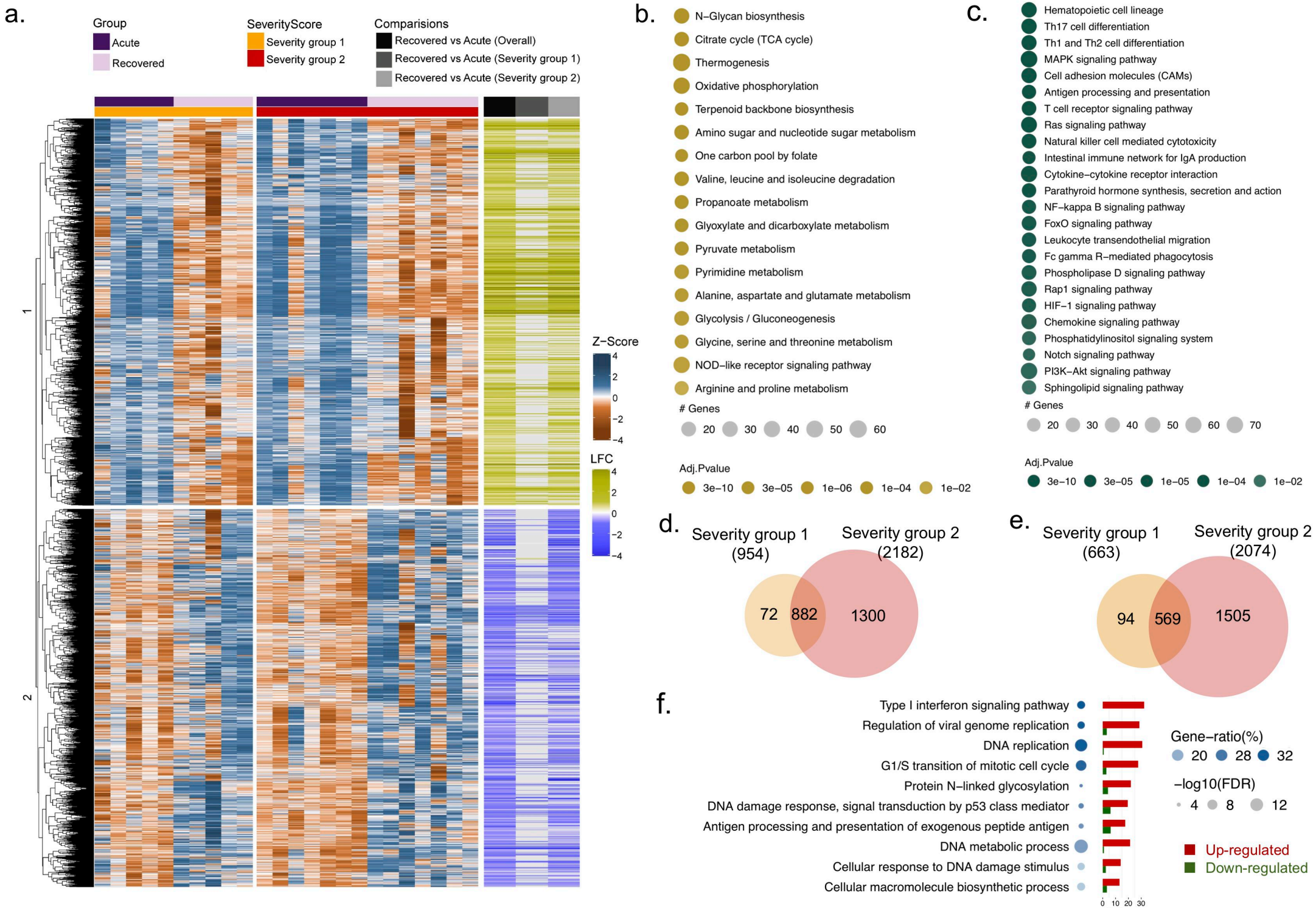
a.
Group
Acute
Recovered
SeverityScore
Severity group 1
Severity group 2
Comparisions
Recovered vs Acute (Overall)
Recovered vs Acute (Severity group 1)
Recovered vs Acute (Severity group 2)
1
2
Z−Score
4
2
0
−2
−4
LFC
4
2
0
−2
−4
b.
N−Glycan biosynthesis
Citrate cycle (TCA cycle)
Thermogenesis
Oxidative phosphorylation
Terpenoid backbone biosynthesis
Amino sugar and nucleotide sugar metabolism
One carbon pool by folate
Valine, leucine and isoleucine degradation
Propanoate metabolism
Glyoxylate and dicarboxylate metabolism
Pyruvate metabolism
Pyrimidine metabolism
Alanine, aspartate and glutamate metabolism
Glycolysis / Gluconeogenesis
Glycine, serine and threonine metabolism
NOD−like receptor signaling pathway
Arginine and proline metabolism
Genes
20 30 40 50 60
Adj.Pvalue
3e−10 3e−05 1e−06 1e−04 1e−02
c.
Hematopoietic cell lineage
Th17 cell differentiation
Th1 and Th2 cell differentiation
MAPK signaling pathway
Cell adhesion molecules (CAMs)
Antigen processing and presentation
T cell receptor signaling pathway
Ras signaling pathway
Natural killer cell mediated cytotoxicity
Intestinal immune network for IgA production
Cytokine−cytokine receptor interaction
Parathyroid hormone synthesis, secretion and action
NF−kappa B signaling pathway
FoxO signaling pathway
Leukocyte transendothelial migration
Fc gamma R−mediated phagocytosis
Phospholipase D signaling pathway
Rap1 signaling pathway
HIF−1 signaling pathway
Chemokine signaling pathway
Phosphatidylinositol signaling system
Notch signaling pathway
PI3K−Akt signaling pathway
Sphingolipid signaling pathway
Genes
20 30 40 50 60 70
Adj.Pvalue
3e−10 3e−05 1e−05 1e−04 1e−02
d.
Severity group 1 (954)
Severity group 2 (2182)
72
882
1300
e.
Severity group 1 (663)
Severity group 2 (2074)
94
569
1505
f.
Type I interferon signaling pathway
Regulation of viral genome replication
DNA replication
G1/S transition of mitotic cell cycle
Protein N−linked glycosylation
DNA damage response, signal transduction by p53 class mediator
Antigen processing and presentation of exogenous peptide antigen
DNA metabolic process
Cellular response to DNA damage stimulus
Cellular macromolecule biosynthetic process
0 10 20 30
% Genes
Gene−ratio(%)
20 28 32
−log10(FDR)
4 8 12
Up-regulated
Down-regulated

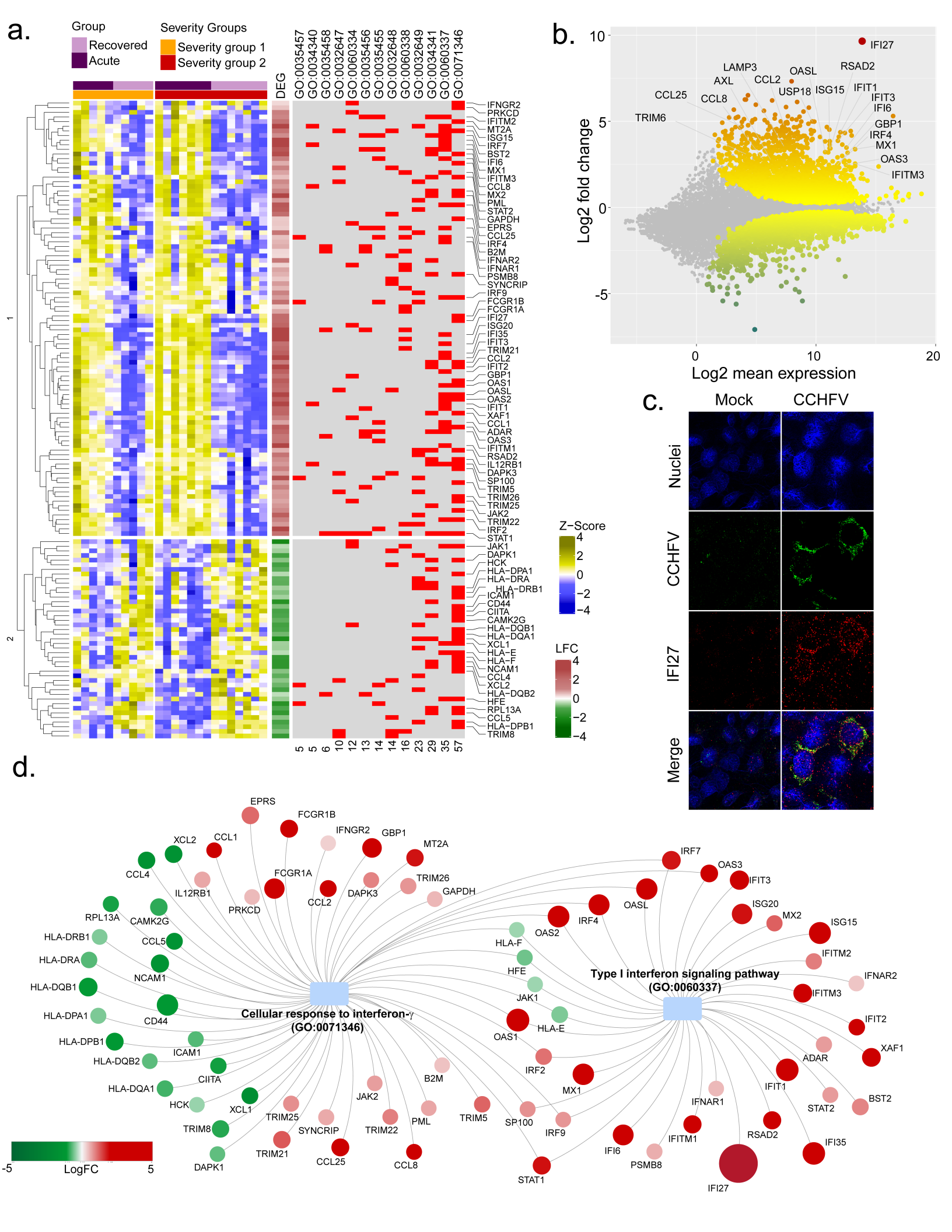
a.
Group
Recovered
Acute
Severity Groups
Severity group 1
Severity group 2
DEG
GO:0035457
GO:0034340
GO:0035458
GO:0032647
GO:0060334
GO:0035456
GO:0035455
GO:0032648
GO:0060338
GO:0032649
GO:0034341
GO:0060337
GO:0071346
IFNGR2
PRKCD
IFITM2
MT2A
ISG15
IRF7
BST2
IFI6
MX1
IFITM3
CCL8
MX2
PML
STAT2
GAPDH
EPRS
CCL25
IRF4
B2M
IFNAR2
IFNAR1
PSMB8
SYNCRIP
IRF9
FCGR1B
FCGR1A
IFI27
ISG20
IFI35
IFIT3
TRIM21
CCL2
IFIT2
GBP1
OAS1
OASL
OAS2
IFIT1
XAF1
CCL1
ADAR
OAS3
IFITM1
RSAD2
IL12RB1
DAPK3
SP100
TRIM5
TRIM26
TRIM25
JAK2
TRIM22
IRF2
STAT1
JAK1
DAPK1
HCK
HLA-DPA1
HLA-DRA
HLA-DRB1
ICAM1
CD44
CIITA
CAMK2G
HLA-DQB1
HLA-DQA1
XCL1
HLA-E
HLA-F
NCAM1
CCL4
XCL2
HLA-DQB2
HFE
RPL13A
CCL5
HLA-DPB1
TRIM8
5
5
6
10
12
13
14
14
16
23
29
35
57
Z-Score
4
2
0
−2
−4
LFC
4
2
0
−2
−4
b.
Log2 fold change
Log2 mean expression
10
5
0
-5
0
10
20
IFI27
LAMP3
OASL
RSAD2
AXL
CCL2
USP18
ISG15
IFIT1
CCL25
CCL8
IFIT3
IFI6
TRIM6
GBP1
IRF4
MX1
OAS3
IFITM3
c.
Mock
CCHFV
Nuclei
CCHFV
IFI27
Merge
d.
Cellular response to interferon-γ
(GO:0071346)
Type I interferon signaling pathway
(GO:0060337)
EPRS
FCGR1B
IFNGR2
GBP1
MT2A
XCL2
CCL1
CCL4
IL12RB1
FCGR1A
CCL2
DAPK3
TRIM26
GAPDH
PRKCD
RPL13A
CAMK2G
HLA-DRB1
CCL5
HLA-DRA
NCAM1
HLA-DQB1
HLA-DPA1
CD44
HLA-DPB1
ICAM1
HLA-DQB2
CIITA
HLA-DQA1
HCK
XCL1
TRIM8
DAPK1
TRIM21
TRIM25
SYNCRIP
CCL25
JAK2
TRIM22
CCL8
PML
B2M
TRIM5
SP100
IRF9
STAT1
IRF7
OAS3
IFIT3
OASL
IRF4
OAS2
ISG20
MX2
ISG15
HLA-F
IFITM2
HFE
IFNAR2
JAK1
IFITM3
HLA-E
OAS1
IFIT2
XAF1
ADAR
IRF2
MX1
IFIT1
IFNAR1
STAT2
BST2
IFITM1
RSAD2
IFI6
IFI35
PSMB8
IFI27
-5
LogFC
5

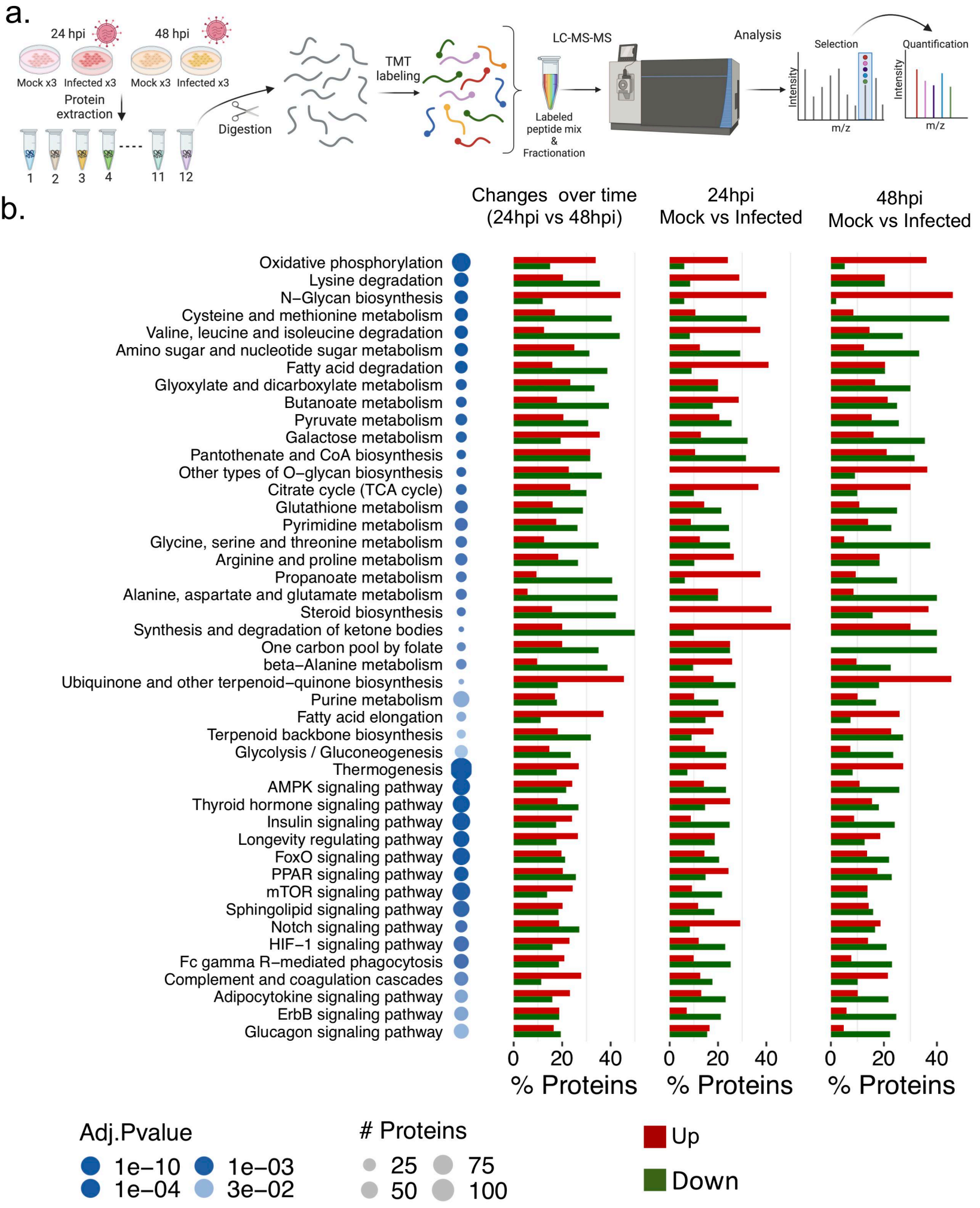
a.
24 hpi
48 hpi
Mock x3
Infected x3
Mock x3
Infected x3
Protein extraction
1
2
3
4
11
12
Digestion
TMT labeling
LC-MS-MS
Labeled peptide mix & Fractionation
Analysis
Selection
Quantification
Intensity
m/z
b.
Changes over time (24hpi vs 48hpi)
24hpi Mock vs Infected
48hpi Mock vs Infected
Oxidative phosphorylation
Lysine degradation
N−Glycan biosynthesis
Cysteine and methionine metabolism
Valine, leucine and isoleucine degradation
Amino sugar and nucleotide sugar metabolism
Fatty acid degradation
Glyoxylate and dicarboxylate metabolism
Butanoate metabolism
Pyruvate metabolism
Galactose metabolism
Pantothenate and CoA biosynthesis
Other types of O−glycan biosynthesis
Citrate cycle (TCA cycle)
Glutathione metabolism
Pyrimidine metabolism
Glycine, serine and threonine metabolism
Arginine and proline metabolism
Propanoate metabolism
Alanine, aspartate and glutamate metabolism
Steroid biosynthesis
Synthesis and degradation of ketone bodies
One carbon pool by folate
beta−Alanine metabolism
Ubiquinone and other terpenoid−quinone biosynthesis
Purine metabolism
Fatty acid elongation
Terpenoid backbone biosynthesis
Glycolysis / Gluconeogenesis
Thermogenesis
AMPK signaling pathway
Thyroid hormone signaling pathway
Insulin signaling pathway
Longevity regulating pathway
FoxO signaling pathway
PPAR signaling pathway
mTOR signaling pathway
Sphingolipid signaling pathway
Notch signaling pathway
HIF−1 signaling pathway
Fc gamma R−mediated phagocytosis
Complement and coagulation cascades
Adipocytokine signaling pathway
ErbB signaling pathway
Glucagon signaling pathway
0
20
40
% Proteins
Adj.Pvalue
1e−10
1e−04
1e−03
3e−02
Proteins
25
50
75
100
Up
Down

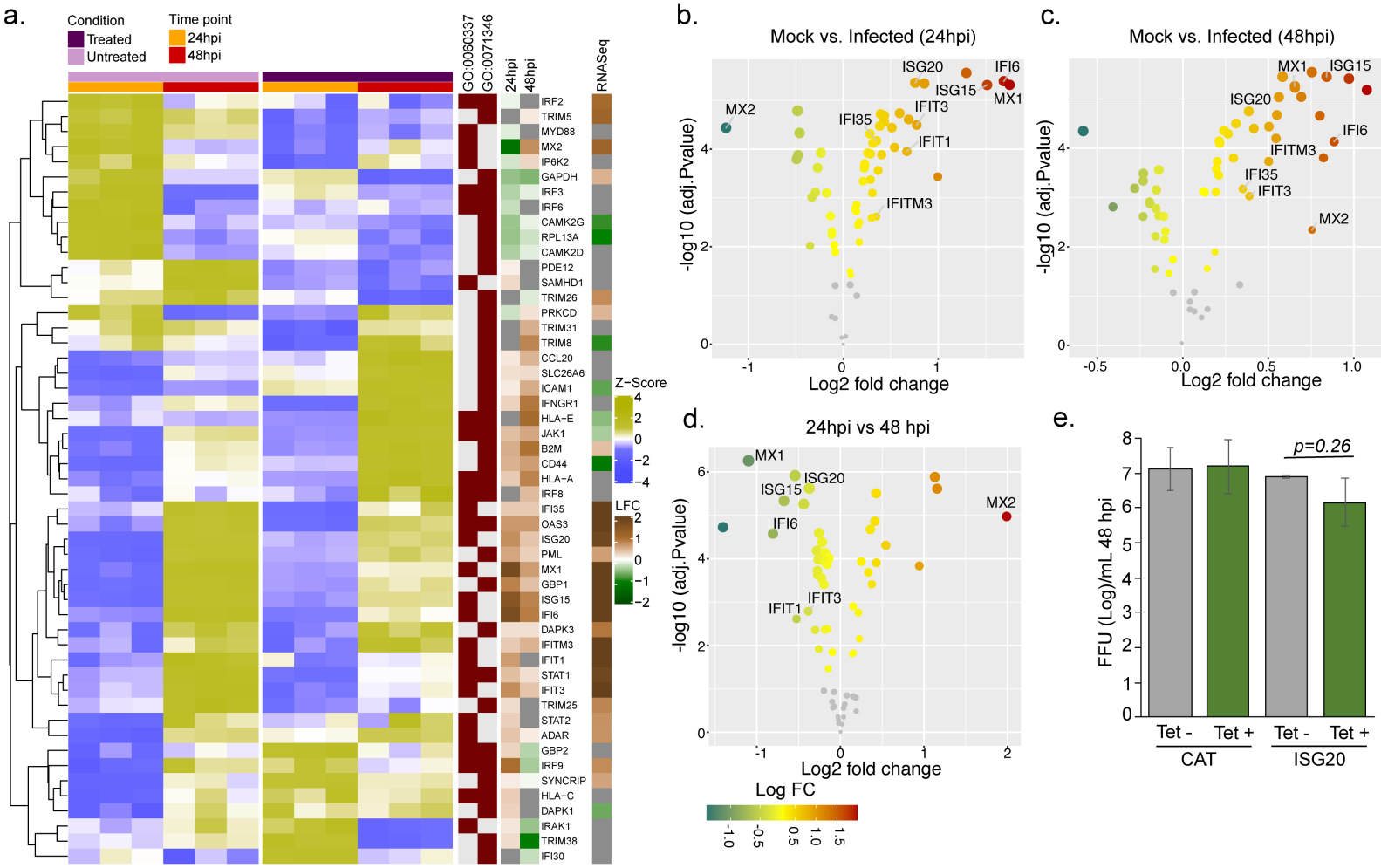
a.
Condition
Treated
Untreated
Time point
24hpi
48hpi
GO:0060337
GO:0071346
24hpi
48hpi
RNASeq
IRF2
TRIM5
MYD88
MX2
IP6K2
GAPDH
IRF3
IRF6
CAMK2G
RPL13A
CAMK2D
PDE12
SAMHD1
TRIM26
PRKCD
TRIM31
TRIM8
CCL20
SLC26A6
ICAM1
IFNGR1
HLA-E
JAK1
B2M
CD44
HLA-A
IRF8
IFI35
OAS3
ISG20
PML
MX1
GBP1
ISG15
IFI6
DAPK3
IFITM3
IFIT1
STAT1
IFIT3
TRIM25
STAT2
ADAR
GBP2
IRF9
SYNCRIP
HLA-C
DAPK1
IRAK1
TRIM38
IFI30
Z-Score
LFC
b.
Mock vs. Infected (24hpi)
-log10 (adj.Pvalue)
Log2 fold change
ISG20
IFI6
ISG15
MX1
IFIT3
MX2
IFI35
IFIT1
IFITM3
c.
Mock vs. Infected (48hpi)
-log10 (adj.Pvalue)
Log2 fold change
MX1
ISG15
ISG20
IFI6
IFITM3
IFI35
IFIT3
MX2
d.
24hpi vs 48 hpi
-log10 (adj.Pvalue)
Log2 fold change
MX1
ISG20
ISG15
IFI6
MX2
IFIT3
IFIT1
Log FC
e.
FFU (Log)/mL 48 hpi
p=0.26
Tet -
Tet +
Tet -
Tet +
CAT
ISG20

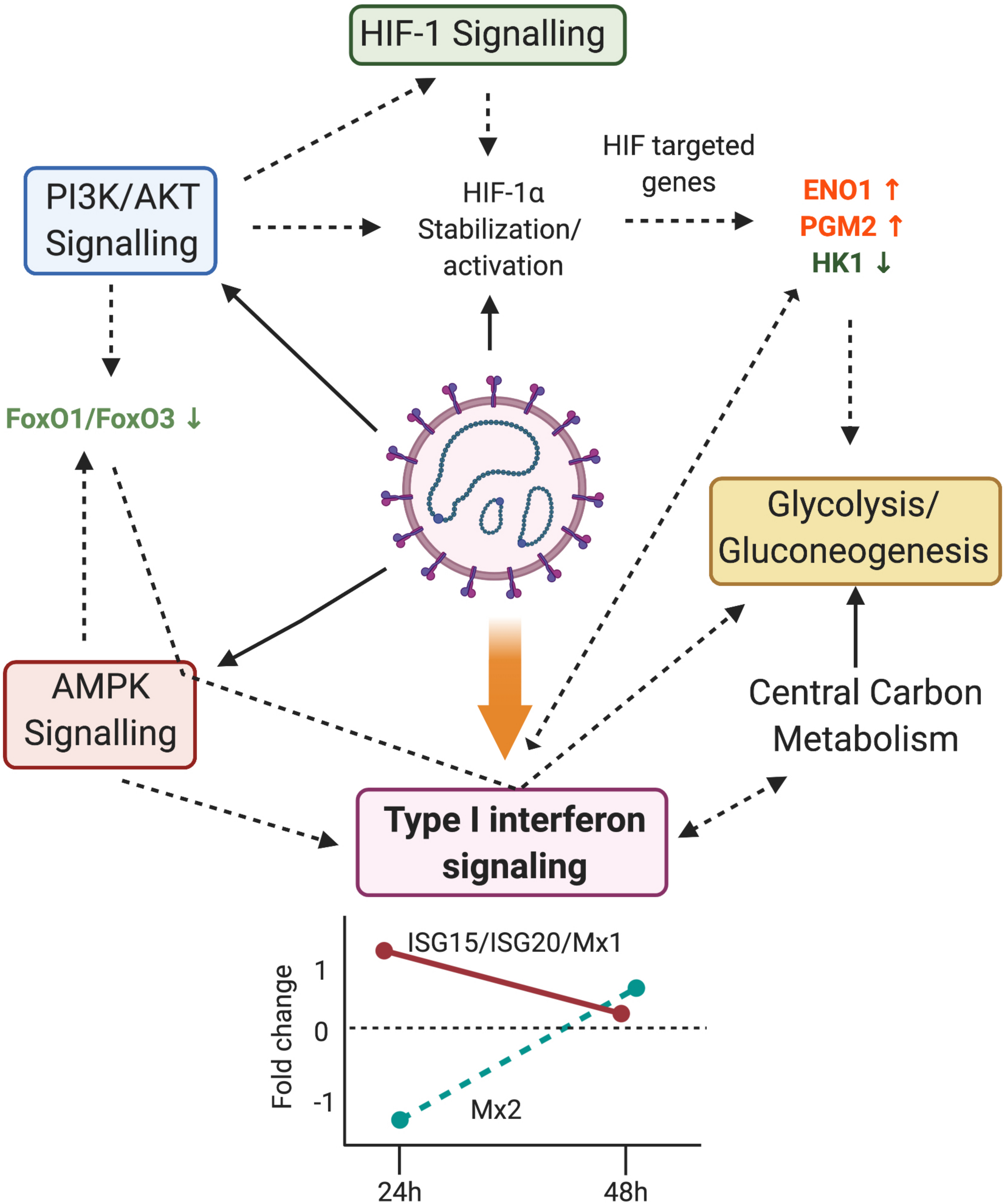
HIF-1 Signalling
PI3K/AKT Signalling
HIF-1α Stabilization/ activation
HIF targeted genes
ENO1 ↑
PGM2 ↑
HK1 ↓
FoxO1/FoxO3 ↓
Glycolysis/ Gluconeogenesis
AMPK Signalling
Central Carbon Metabolism
Type I interferon signaling
ISG15/ISG20/Mx1
Mx2
Fold change
1
0
-1
24h
48h